Biomaterials Science

ROYAL SOCIETY OF CHEMISTRY

PAPER

View Article Online
View Journal | View Issue

Open Access Article. Published on 31 July 2024. Downloaded on 10/30/2025 4:59:12 PM.
This article is licensed under a Creative Commons Attribution 3.0 Unported Licence.

Check for updates

Cite this: *Biomater. Sci.*, 2024, **12**, 4695

Impact of morphological features and chemical composition of tendon biomimetic scaffolds on immune recognition *via* Toll-like receptors

Sara Gil-Cantero,[a,b] Francesco Iorio,[b] Irem Unalan,[b] Fatih Kurtuldu,[c] Sarojinidevi Künig,[a] Claus Wenhardt,[a] Veronica Pinnaro',[a] Katharina Aigner-Radakovics,[a] Peter Steinberger,[a] Aldo R. Boccaccini *[b] and Johannes Stöckl *[a]

Tendinopathies are a major worldwide clinical problem. The development of tendon biomimetic scaffolds is considered a promising, therapeutic approach. However, to be clinically effective, scaffolds should avoid immunological recognition. It has been well described that scaffolds composed of aligned fibers lead to a better tenocyte differentiation, vitality, proliferation and motility. However, little has been studied regarding the impact of fiber spatial distribution on the recognition by immune cells. Additionally, it has been suggested that higher hydrophilicity would reduce their immune recognition. Herein, polycaprolactone (PCL)–hyaluronic acid (HA)-based electrospun scaffolds were generated with different fiber diameters (in the nano- and micro-scales) and orientations as well as different grades of wettability and the impact of these properties on immunological recognition has been assessed, by means of Toll-like receptor (TLR) reporter cells. Our results showed that TLR 2/1 and TLR 2/6 were not triggered by the scaffolds. In addition, the TLR 4 signalling pathway seems to be triggered to a greater extent by higher PCL and HA concentrations, but the alignment of the fibers prevents the triggering of this receptor. Taken together, TLR reporter cells were shown to be a useful and effective tool to study the potential of scaffolds to induce immune responses and the results obtained can be used to inform the design of fibrous scaffolds for tendon repair.

Received 26th January 2024,
Accepted 19th May 2024

DOI: 10.1039/d4bm00147h

rsc.li/biomaterials-science

1. Introduction

Tendons are connective tissue, mainly composed of collagen type I. These proteins show a hierarchical organisation which leads to fibers of greater thickness and aligned spatial distribution.[1] This disposition of the fibers is essential for tendons to perform their function: transmitting the forces from the muscle to the bone, enabling body movement. In order to accomplish this purpose, tendons need to withstand high mechanical stresses.[2–7]

Excessive mechanical stress, as well as other factors such as diseases, genetics or epigenetics, might lead to tendinopathies.[8,9] These processes are characterised by an inflammatory phase, where the extracellular matrix (ECM) is degraded and pro-inflammatory molecules are released. It is followed by a regenerative phase, characterised by the deposition of new collagen units and the expression of anti-inflammatory molecules.[2,8,10] During this second phase, collagen type III is the main subtype produced, which shows lower mechanical properties than collagen type I.[2,11,12] It is deposited in a disorganized disposition, which leads to scar formation and loss of function.[4,13,14] Due to the poor cellularization and vascularization of this tissue, the regeneration of the tendons is slow and the inflammatory phase tends to become chronic.[14,15] As a result, these conditions are associated with pain, loss of tendon functionality and reduced mobility of the affected region. Tendinopathies have a high impact on society from both a clinical and an economic perspective, as they affect millions of people worldwide.[8,16,17]

In this context, the development of scaffolds based on biopolymers is one of the most promising therapeutic approaches.[18] These scaffolds biomimic the aligned tendon structure based on collagen fibers, substituting the defective tissue while it regenerates, and supporting cellular growth.[4,16] One of the most promising techniques used to produce

[a]*Center for Pathophysiology, Infectiology and Immunology, Institute of Immunology, Medical University of Vienna, Vienna, Austria.*
E-mail: johannes.stoeckl@meduniwien.ac.at
[b]*Institute of Biomaterials, Department of Materials Science and Engineering, University of Erlangen-Nuremberg, Germany. E-mail: aldo.boccaccini@fau.de*
[c]*FunGlass, Alexander Dubček University of Trenčín, Trenčín, Slovakia*

Open Access Article. Published on 31 July 2024. Downloaded on 10/30/2025 4:59:12 PM. This article is licensed under a Creative Commons Attribution 3.0 Unported Licence.

fibrous scaffolds is electrospinning (ES).[4] ES is a very versatile method, which enables the use of different polymers and solvents, as well as obtaining scaffolds with different morphological characteristics that can mimic the native tendon tissue structure.[4,19–22] Therefore, research is currently highly focused on this strategy and different electrospun fibers composed of natural and/or synthetic polymers have been developed.[4,16,23–25] Functionalization with different cells or molecules has been performed and the suitability of the fibrous structures for tendon regeneration purposes has been studied.[26–28]

The immune recognition of the scaffold is a key step for the immune response and inflammation. The latter might take place as a result of recognising the scaffold as a foreign body.[29–33] Among the different immunological receptors involved in the early stages of the innate immune response, Toll-like receptors (TLRs) constitute one of the most important sensors expressed both in the cellular surface membrane and intracellularly. They recognise a wide variety of ligands.[34] Their activation has been suggested as plasma proteins adsorb to the scaffolds after implantation and they expose antigenic sites, which bind TLRs.[35–37] As a result, neutrophils, monocytes, macrophages and dendritic cells, which express those receptors, are activated and initiate inflammation.[31,32,38–40] This process can lead to macrophage fusion into giant body cells and the activation of fibroblasts, which produce a fibrotic capsule to isolate the implanted biomaterial.[31,32,36] This immunological recognition has, therefore, an essential impact on the outcome of the therapeutic approach and its research is hence vital.[32,33] However, there is still a lack of understanding about it and its *in vitro* assessment is still unable to predict the host response to the biomaterial.[30,41–43]

Polycaprolactone (PCL) is a synthetic polymer highly used in tissue engineering. It is inexpensive, biocompatible, and biodegradable and it shows a low degradation rate and great versatility regarding the type of scaffolds that can be produced as well as the postproduction modifications.[44–46] These characteristics, together with its mechanical properties, make it a suitable component for tendon tissue engineering.[46] However, PCL shows low hydrophilicity, reducing the cellular attachment as well as increasing the protein adsorption and inflammatory response after scaffold implantation.[46–54] Therefore, its combination with a second component which enables an increase in the wettability of the final product is essential.

Hyaluronic acid (HA) is a highly hydrophilic glycosaminoglycan, naturally present in the ECM.[55] Additionally, it has also been described to prevent microbial colonisation,[56] as well as to improve cellular viability and collagen type I production without enhancing the expression of collagen type III in tendons.[57] Hence, it is an excellent hydrophilic component to apply in tendon tissue engineering.

The impact of some biomaterial properties (*e.g.*, surface roughness and pore size) on immune cells (*e.g.*, dendritic cells) has been superficially analysed.[33] Besides, the effect of the scaffold morphological features on the target tissue cells has been previously studied. Wu *et al.* demonstrated that mimicking the alignment of the collagen fibers favours tenogenic differentiation as well as cell infiltration, orientation and proliferation, in comparison with those that show a random spatial distribution.[58] Additionally, thicker fibers were found to enhance the proliferation of different cell types.[59–62] Furthermore, some studies have been carried out to understand how these features impact macrophage polarization and cytokine production.[38,40] However, to the best of our knowledge, it has not been addressed yet how these characteristics affect immune cell recognition of the scaffolds. Moreover, an analytical tool that enables addressing this interplay for different innate immune cells at once and with a simple and fast read out has not been described yet.

This study aims to determine how the morphology of fibrous scaffolds affects their immunological recognition. For that purpose, we produced and characterized electrospun scaffolds (Fig. 1) with different fiber diameters, varying PCL concentrations and two different spatial distributions, random and aligned, by using two different collectors. Additionally, different concentrations of HA were also included in order to decrease the hydrophobicity of PCL. Concerning the assessment of scaffold immunological recognition, we have used a novel cellular tool constituted by TLR reporter cells,[63,64] human Jurkat-based cells that express TLRs.

2. Materials and methods

2.1 Materials

Polycaprolactone (PCL, average M_n 80 000); acetic acid glacial (AA, ReagentPlus®, >99%); fetal bovine serum (FBS); and cell counting kit-8 (WST-8) were purchased from Sigma Aldrich (Darmstadt, Germany). RPMI 1640 medium; phorbol 12-myristate 13-acetate, 12-*O*-tetradecanoylphorbol 13-acetate (PMA); and propidium iodide were acquired from Sigma-Aldrich (St Louis, MO, USA). Hyaluronic acid sodium salt (molecular weight 80 000–100 000 kDa) was obtained from Carbosynth Ltd (UK). Formic acid (FA, 98%) was purchased from GPR Reactapur (UK). Dulbecco's phosphate buffered saline (DPBS); Dulbecco's Modified Eagle's Medium (DMEM) 1 g L^{-1} D-glucose; pyruvate (DMEM); trypsin/EDTA; blue 4′,6-diamidino-2-phenylindole, dilactate (DAPI); and rhodamine-phalloidin were ordered from Invitrogen, Thermo Fisher Scientific (Schwerte, Germany). L-Glutamine; penicillin; and streptomycin were acquired from Invitrogen, Thermo Fisher Scientific (Schwerte, Germany) and Gibco Ltd (Paisley, UK). Normal human dermal fibroblasts (NhDFs) were procured by Promo Cell (Heidelberg, Germany) and the Dermatology Clinic of Medical University of Vienna (MUW). The experiments were performed in accordance with the principles of the Declaration of Helsinki and approved by the MUW Ethics Committee. Written consent was obtained from the participants (Vote no.: 1149/2011: isolation and culture of cells and analysis of normal human skin biopsies). TLR reporter cells are Jurkat based cells which express the green fluorescent protein (GFP) under the control of an NFkß promoter. They

 This journal is © The Royal Society of Chemistry 2024

Open Access Article. Published on 31 July 2024. Downloaded on 10/30/2025 4:59:12 PM.
This article is licensed under a Creative Commons Attribution 3.0 Unported Licence.

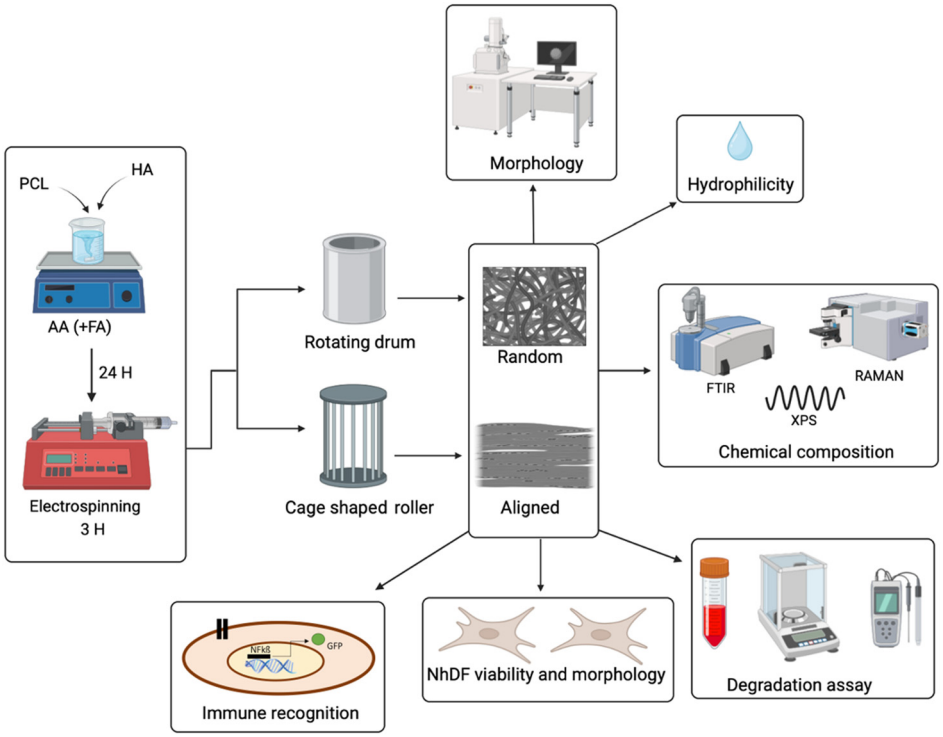

Fig. 1 Experimental design. Production, characterization and immune recognition of tendon biomimetic electrospun scaffolds, which show different fiber diameters and orientations. Image produced with Biorender© software.

only express the indicated TLR. They were generated at the Institute of Immunology, Medical University of Vienna (Vienna, Austria) as previously described.[63,64]

2.2 Production of electrospun PCL-HA-based tendon biomimetic scaffolds

Based on published data and methods,[65–70] different parameters were tested. The protocol for PCL–HA-based electrospun scaffolds performed in this study was determined according to the electrospinnability, uniformity and beadless formation of the scaffolds, together with an appropriate fiber spatial distribution. Briefly, PCL pellets (12 or 20%) and HA powder (0, 0.5 or 0.75%) were dissolved in an AA/FA 1 : 1 or AA pure solvent, respectively. After 24 h of stirring at room temperature (RT), the solutions were loaded in different 3 mL plastic syringes. Subsequently, the solutions were electrospun using a commercial electrospinning device (IME's medical electrospinning machines, EC-16 CLI, IME Technologies, Netherlands) under a constant temperature (25 °C) and relative humidity (25%). Additionally, −1 kV was applied to the target and +14 kV to the 23G needle, while the solution was fed at a constant flow rate (0.4 mL h^{-1}). Two different collectors were placed at 11 cm distance from the needle, in order to obtain two different spatial distributions of the fibers: a rotating drum collector, which was wrapped with an aluminium sheet, for random fibers and a cage shaped roller collector with 2 cm distance between the metallic bars and with 17 × 0.5 cm aluminium straps placed along the metallic bars to favour the collection of the fibers.

2.3 Characterisation of the scaffolds

The morphology of the scaffolds was analysed by scanning electron microscopy (SEM, ETH: 0.5 kV, Everhart–Thornley detector (SE2), AURIGA base 55, Carl Zeiss, Oberkochen, Germany). For that purpose, a SEM holder was covered with a double carbon tape and, subsequently, a small segment of the scaffold was cut and placed on top. The average and standard deviation regarding the fiber diameter were obtained by measuring 50 randomly selected fibers from SEM images, using ImageJ software. Alignment was also analysed with the latter.

The porosity of the scaffolds was measured using ImageJ software, following the flowchart previously described.[71]

Hydrophobicity was determined *via* the measurement of the contact angle of the scaffolds. After placing the samples between two glass slides, 10 μL of dH_2O were dropped on the scaffold's surface and the contact angle was measured using a contact angle meter (DSA30 CA Measurement setup, Kruess GmbH). The procedure was repeated 3 times in different positions of the same scaffold and the average and standard deviation were then calculated.

The chemical composition of the scaffolds was analysed by Fourier-transform infrared spectroscopy (FTIR), Raman spectroscopy and X-ray photoelectron spectroscopy (XPS). FTIR analyses were carried out using a Spectrum™ 3 FT-IR spectro-

Open Access Article. Published on 31 July 2024. Downloaded on 10/30/2025 4:59:12 PM. This article is licensed under a Creative Commons Attribution 3.0 Unported Licence.

meter (PerkinElmer, USA) in the wavenumber range from 4000 to 250 cm^{-1} at a resolution of 4 cm^{-1} using 45 scans per sample. Raman spectra were collected in 100–3200 cm^{-1} wavenumber range, using a Raman spectrometer (Renishaw inVia Reflex, UK). A semiconductor (λ = 532 nm) laser with 15 s of exposure time was used. For XPS measurements, a Nexsa G2 Thermo-Scientific, monochromated Al Kα radiation and a spot size of 400 μm were used. The survey spectra were acquired in the binding energy range of 0–1350 eV with an energy step size of 1 eV and a pass energy of 200 eV. High-resolution elemental XPS data were obtained using an energy step size of 0.1 eV and a pass energy of 50 eV.

2.4 Scaffold stability

For assessing the stability of the samples, a 6 cm × 2 cm piece of each scaffold was weighed and sterilised 45 minutes under UV light. Then, the scaffolds were immersed in DMEM 1 g mL^{-1} glucose, enriched with FBS (10%) and streptomycin/penicillin (1%), keeping a mg mL^{-1} ratio of 1 : 1. After incubating them at 37 °C and 90 rpm for 48 h, pH of the medium was measured using a pH meter (FiveEasy Plus pH-meter FB20, Giessen, Germany) and the scaffolds were collected and dried for 2 days at 37 °C and 90 rpm. Scaffolds were then weighed again and the degradation was calculated as the loss of weight (%). The pH variation was calculated as the difference between the samples and the mean of 3 controls whose pH values were measured under the same conditions.

2.5 NhDF seeding and culture

DMEM 1 g mL^{-1} glucose supplemented with FBS (10%) and penicillin/streptomycin (1%) was used to culture the NhDFs in 75 cm^2 cell culture flasks (Nunc, Denmark) until confluency. Cells were subsequently detached by adding 5 mL of acutase at 37 °C for 10 minutes. An automated cell counter system (Beckman Coulter Z2 Particle Counter, Vienna, Austria) was used to count the cells. Then, scaffolds were placed on CellCrown 24 inserts (ScaffedexOy, Tampere, Finland) and sterilised 45 min per side under UV light. 1 mL of media was used to condition the scaffolds for 30 minutes. Afterwards, 15,000 cells in 20 μL were cultured on top of the scaffolds per well and incubated at 37 °C, 5% CO_2, 80% relative humidity (RH) for 2 h to let the cells attach to the scaffolds. Finally, DMEM was added up to 500 μL per well and plates were incubated for 1, 3, 7 and 14 days.

2.6 NhDF proliferation

At the different time points, samples were washed with PBS 1× twice and transferred to a new plate. Then, 1% WST was added for 3 h. Negative control (blank), consisting of DMEM with no cells, and positive control, consisting of cells without scaffolds, were also included. Subsequently, absorbance was measured at 450 nm using a microplate reader (Microplate Photometer HiPo MPP-96, Riga, Latvia). Proliferation was calculated normalising the data against the day 1 measurement.

2.7 NhDF morphology on the scaffolds

In order to visualise the morphology of cells attached to the scaffolds, rhodamine-phalloidin/DAPI staining was carried out. Briefly, samples were washed with PBS after the proliferation analysis and 500 μL of Flofix (2.8% glutaraldehyde) was added. After 15 minutes incubation at RT, samples were washed with PBS. Then, 500 μL of permeabilization buffer was added and incubated at RT for 5 minutes. After removing the permeabilization agent, 500 μL of 8 μL mL^{-1} phalloidin was added and incubated at RT for 45 minutes. Samples were washed with PBS and 500 μL of DAPI was added and incubated at RT for 5 minutes. Finally, samples were washed with PBS and kept at 4 °C immersed in 1 mL of PBS upon image capture with a fluorescence microscope (DMI 6000B, Leica, Germany).

2.8 TLR reporter cell activation *via* scaffolds

RPMI supplemented with FBS (10%), penicillin/streptomycin (1%) and L-glutamine (1%) was used to culture the TLRs (TLR 2/1, TLR 4 and TLR 2/6) in 25 cm^2 cell culture flasks (Nunc, Denmark). Cells were subsequently collected and counted, by using an automated cell counter system (Beckman Coulter Z2 Particle Counter, Vienna, Austria). Scaffolds were placed on CellCrown 24 inserts (ScaffedexOy, Tampere, Finland) and sterilised 45 min per side under UV light. 500,000 cells in 100 μL were cultured on top of the scaffolds per well in 24 well plates. RPMI was added up to 500 μL per well and incubated at 37 °C, 5% CO_2, 80% RH for 24, 48 and 72 hours. Negative controls with just the cells were also included. A positive control for TLR reporter cell triggering was included by adding 100 nM PMA.

At the different time points, the mean fluorescence intensity (MFI) of the expressed GFP by the triggered TLR reporter cells and their viability were measured. Briefly, 100 μL of the cells per well were centrifuged and washed with PBS 1× enriched with FBS (1%). Subsequently, 50 μL of 100 ng mL^{-1} propidium iodide was added. Finally, GFP and propidium iodide MFIs were measured using a FACS Calibur flow cytometer (BD Biosciences).

2.9 Statistical analysis

Statistical analyses were performed using Prism version 9.4.0. The influence of any of the three studied factors (PCL concentration, HA concentration and alignment) was analysed by three-way ANOVA tests. *Post hoc*, pairwise Tukey's *t*-tests were performed.

3. Results and discussion

3.1. Analyzing the surface morphology of the scaffolds used in this study

In order to investigate how the different morphological features of the tendon biomimetic scaffolds have an impact on the immune recognition, specimens with different morphological characteristics were produced. The main physical fea-

 This journal is © The Royal Society of Chemistry 2024

Open Access Article. Published on 31 July 2024. Downloaded on 10/30/2025 4:59:12 PM.
This article is licensed under a Creative Commons Attribution 3.0 Unported Licence.

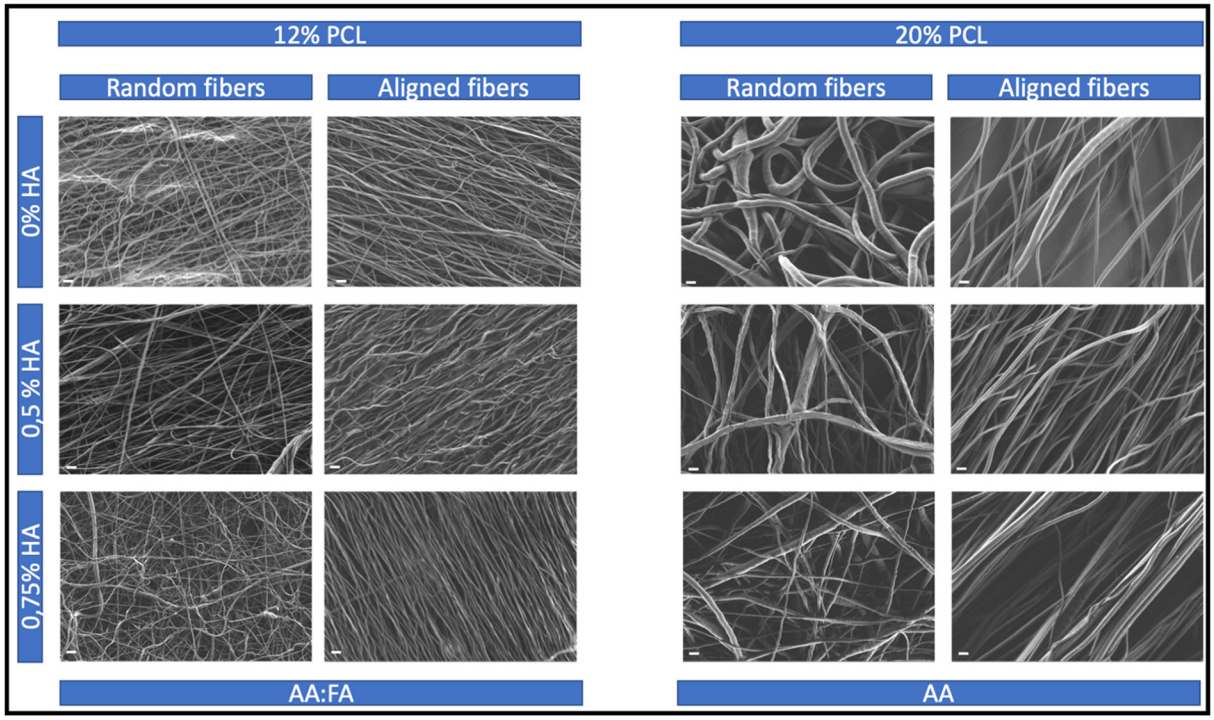

Fig. 2 Scaffold morphology. Scanning electron microscopy (SEM) images from the 12 different specimens produced. PCL: polycaprolactone; HA: hyaluronic acid; AA: acetic acid; FA: formic acid. Scale bar: 2 μm.

tures whose impact was investigated were the fiber diameter and the alignment of the fibers, the latter being essential for tendon tissue regeneration.[4,16]

As a result of varying the PCL and HA concentrations, as well as the solvent system and the use of different collectors, 12 different scaffolds were produced. As can be observed in Fig. 2, all the specimens were uniform and bead-free.

The increase of the fiber diameter was significantly achieved by increasing the concentration of PCL and changing the solvent system (Fig. 3A), transitioning from nano- to micrometers (Table 1). Generally, an increase in the polymer concentration leads to the formation of fibers with higher diameters as there is more polymer available.[72] Additionally, the more volatile the solvent, the quicker it evaporates, the more stretching is applied to the fibers and the smaller their diameter.[73,74] As AA shows a higher boiling point (117.9 °C) than FA (101 °C),[75] in this case, the higher fiber diameter of the 20% PCL scaffolds was the result of applying not only a higher concentration of PCL but also a less volatile solvent system.

For the scaffolds with random distribution of the fibers, it can be observed that the addition of HA led to an increase in the fiber diameter when composed of 12% PCL, while having the opposite, significant effect in the 20% PCL random scaffolds. The HA used for the generation of the scaffolds is a sodium salt and salts have been previously described to increase the conductivity and the charge present in the fluid surface.[74] The latter results in a greater stretching of the fibers and, therefore, in smaller fiber diameters.[76–78] This might be

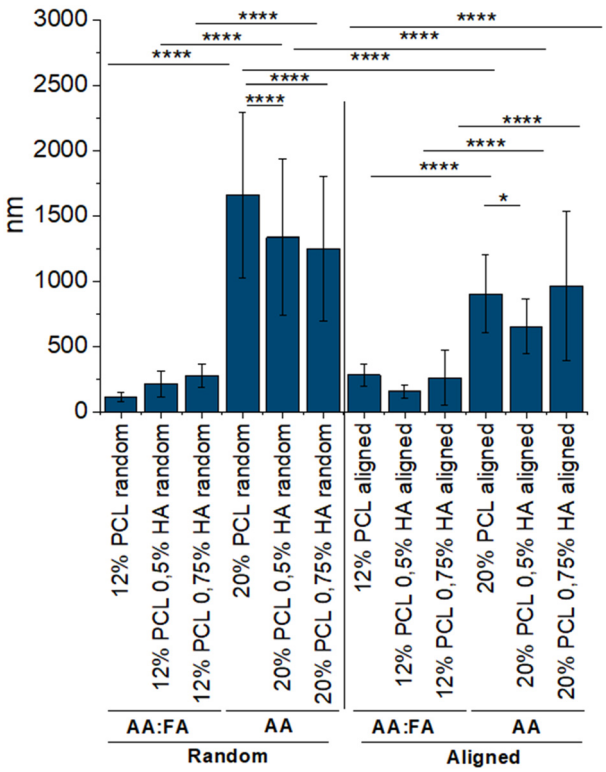

Fig. 3 Fiber diameter. Comparison of the scaffolds' fiber diameter, measured on SEM images using ImageJ software. PCL: polycaprolactone; HA: hyaluronic acid; AA: acetic acid; FA: formic acid; nm: nanometer. Data are shown as mean ± SEM (n = 50). Two-way ANOVA test with $p^* < 0.05$; $p^{****} < 0.0001$.

Open Access Article. Published on 31 July 2024. Downloaded on 10/30/2025 4:59:12 PM.
This article is licensed under a Creative Commons Attribution 3.0 Unported Licence.

Table 1 Summary of morphological features. PCL and HA concentrations, as well as orientation of the fibers and their diameters are presented. Data are shown as mean ± SD (n = 50). PCL: polycaprolactone; HA; hyaluronic acid; AA: acetic acid; FA: formic acid; nm: nanometer; w/w: percentage in weight

Specimen	Solvent(s)	PCL (w/w)	HA (w/w)	Orientation	Fiber diameter (nm)	Porosity (%)
1	AA : FA	12	0	Random	114 ± 39	27 ± 2
2	AA : FA	12	0.5	Random	213 ± 96	28 ± 1
3	AA : FA	12	0.75	Random	274 ± 87	22 ± 3
4	AA	20	0	Random	1663 ± 630	18 ± 1
5	AA	20	0.5	Random	1336 ± 593	17 ± 2
6	AA	20	0.75	Random	1250 ± 545	21 ± 3
7	AA : FA	12	0	Aligned	280 ± 87	28 ± 2
8	AA : FA	12	0.5	Aligned	156 ± 45	22 ± 1
9	AA : FA	12	0.75	Aligned	243 ± 173	13 ± 2
10	AA	20	0	Aligned	903 ± 296	26 ± 2
11	AA	20	0.5	Aligned	654 ± 209	15 ± 1
12	AA	20	0.75	Aligned	964 ± 564	21 ± 4

the reason for observing thinner fibers when increasing the HA concentration in the 20% PCL scaffolds, a phenomenon that was also previously reported.[79,80] However, for the 12% PCL scaffolds, the presence of FA in the solvent system might lead to a different conductivity, resulting in the opposite result.

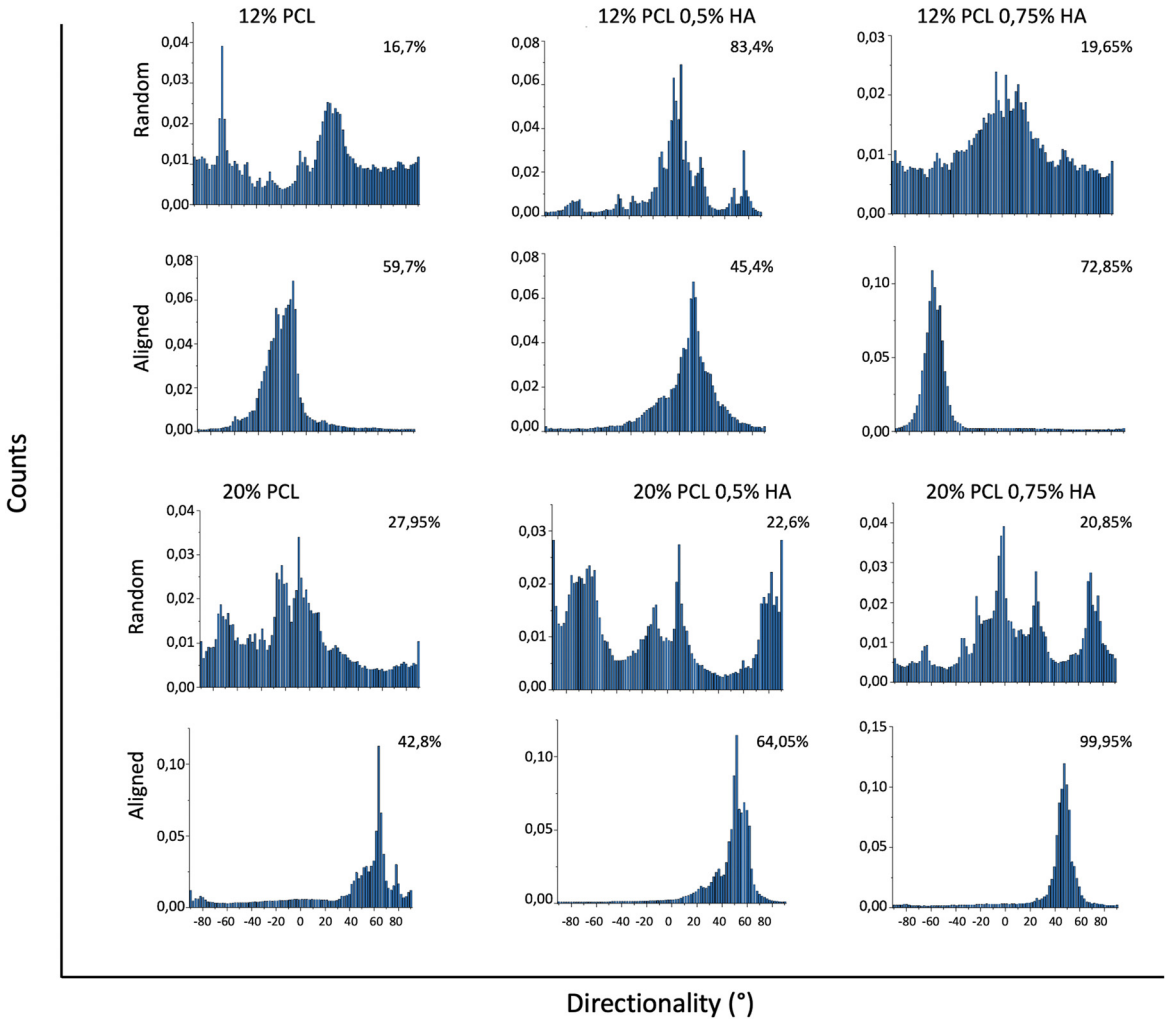

Fig. 4 Alignment of fibers. Directionality of the scaffolds' fibers processed by ImageJ software. Data are shown as percentage of alignment within −10° and +10°. PCL: polycaprolactone; HA: hyaluronic acid.

 This journal is © The Royal Society of Chemistry 2024

Open Access Article. Published on 31 July 2024. Downloaded on 10/30/2025 4:59:12 PM.
This article is licensed under a Creative Commons Attribution 3.0 Unported Licence.

Regarding the aligned biomaterials, alignment led to a significant reduction of the fiber diameter when comparing these specimens to their random distributed equivalents (Fig. 3B). Collector rotation speed has been previously described to improve the alignment of the fibers while decreasing their diameter.[81] However, in this set up, both random and aligned fibers were produced using the same rotation speed. The only parameter that differed was the type of collector, a parameter that has also been described to have an effect on the morphological features.[82] A rotating drum was used for the random fibers but for aligned ones the choice was a cage shaped roller collector, and it might be speculated that the disposition of the metallic bars within the latter might subject the fibers to a higher stretching, leading to smaller diameters.

The addition of HA greatly increased fiber orientation, especially for specimens with higher concentrations of PCL (Fig. 4). This behavior might be due to different reasons: firstly, a higher concentration of polymer is usually linked with higher viscosity values,[74] a parameter that enables a better stretching of the fibers due to a lower tendency to be deformed.[83] This greater stretching results in a better alignment, which is observed in the 20% PCL scaffolds in comparison with the 12% PCL ones. Secondly, the increase in HA concentration leads to a higher surface charge density of the fluid, as mentioned above, which also results in a better stretching. Therefore, the more the HA, the more is the alignment obtained. In the 20% PCL 0.75% HA specimens, hence, the alignment was the highest because of the combination of both factors.

Beyond the fiber diameter and spatial distribution, the pore size is also a morphological characteristic to be considered for tissue engineering purposes. It has been previously described to influence cell differentiation, attachment and growth, as well as scaffold degradation.[84] Fiber diameter has been described to have a direct impact in the porosity of the scaffolds, by reducing the value of the latter upon thicker fiber formation. However, other electrospinning parameters, such as the viscosity and conductivity, may also affect this feature.[85,86] As shown in Fig. 5, and summarised in Table 1, the different parameters applied for the generation of the scaffolds used in this study had a different impact on the porosity. The presence of FA in the solvent system led to scaffolds

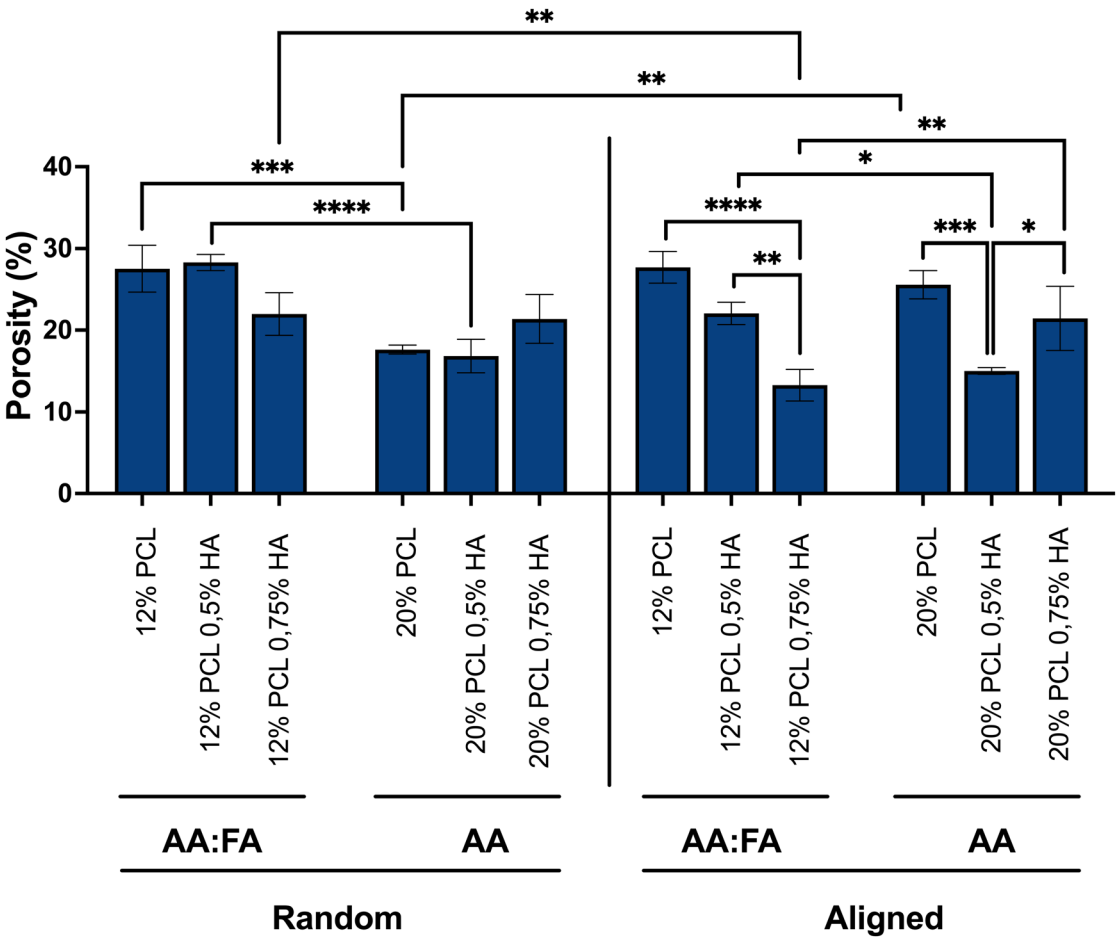

Fig. 5 Porosity. The porosity (%) of the different scaffolds, obtained using ImageJ software, are presented. nm: nanometer. Data are shown as mean ± SEM (n = 3). Three-way ANOVA test with $p^{*} < 0.05$; $p^{**} < 0.01$; $p^{***} < 0.001$; $p^{****} < 0.0001$. PCL: polycaprolactone; HA: hyaluronic acid; AA: acetic acid; FA: formic acid.

Open Access Article. Published on 31 July 2024. Downloaded on 10/30/2025 4:59:12 PM.
This article is licensed under a Creative Commons Attribution 3.0 Unported Licence.

with lower porosity upon higher HA concentration. However, for the scaffolds where only AA was used, the impact of HA concentration on porosity followed no trend. Additionally, a higher PCL concentration leads to lower porosity values, which correlates to the studies mentioned above. Furthermore, alignment which reduced the fiber diameter and, thus, would increase the porosity according to those studies, led in this case, to opposite results depending on PCL concentration. Samples with 12% PCL presented a decrease in porosity while specimens composed of 20% PCL showed an increase in this parameter, when fibers are aligned. As explained above, the presence of salts, different solvents and different polymer concentrations influence the charge density, viscosity and evaporation rate, leading to different fiber stretching and deposition. Moreover, the collector used for obtaining the scaffolds also has an effect on the latter. Therefore, all these parameters and their variations not only impacted the fiber diameter and alignment, but also the scaffold porosity.

3.2. Analyzing the chemical properties of the scaffolds used in this study

Physical, chemical and biological characteristics of the scaffolds play a crucial role in determining the cellular behavior in the context of tissue engineering for tissue regeneration.[49] Within the chemical features, hydrophilicity is one of the essential parameters of biomaterial surfaces.

Taking into consideration that PCL has low hydrophilicity, the addition of a hydrophilic component into the scaffolds was thought to be critical. HA is a highly hydrophilic glycosaminoglycan, naturally present in the ECM,[55] which has previously shown beneficial effects for tendon regeneration.[55–57] Nevertheless, due to its negative charge, it is difficult to electrospin HA if it is not further modified.[87] Indeed, scaffolds with 1% HA could not be produced. As a result, 0.5 and 0.75% HA were chosen.

To demonstrate the incorporation of the HA into the scaffolds, FTIR and Raman analysis were performed but no differences in the spectra were observed (data not shown), in spite of the existence of other studies showing their capability to detect and distinguish HA.[88–91] Therefore, an XPS analysis was carried out.

As shown in Fig. 6, the scaffolds with HA showed a sodium (Na) peak. This result provided evidence of HA integration into the scaffold as the reagent used was a HA sodium salt. Additionally, the 12% PCL 0.75% HA specimen (representative scaffold used for the analysis) showed more intense carbon (C) and oxygen (O) peaks, which is likely due to the presence of these atoms also in the HA molecule.

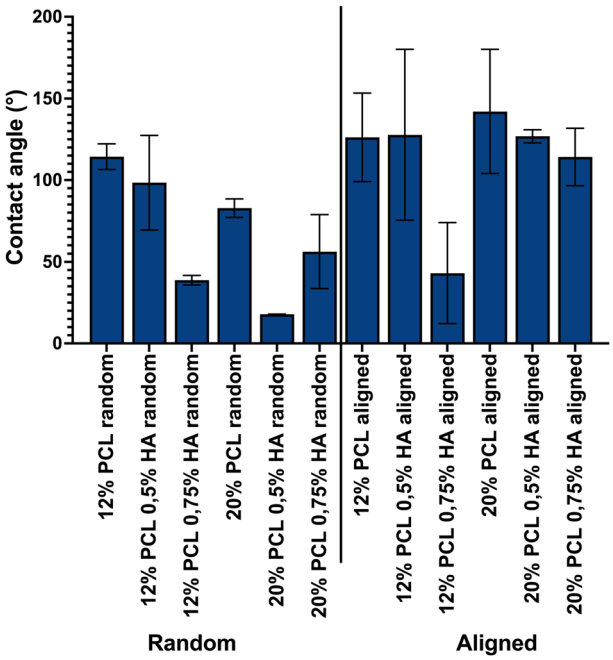

Fig. 7 Hydrophobicity. Wettability of the scaffolds measured by the contact angle technique. PCL: polycaprolactone; HA: hyaluronic acid. Data shown as mean ± SEM (n = 3). Two-way ANOVA test with $p^* < 0.05$.

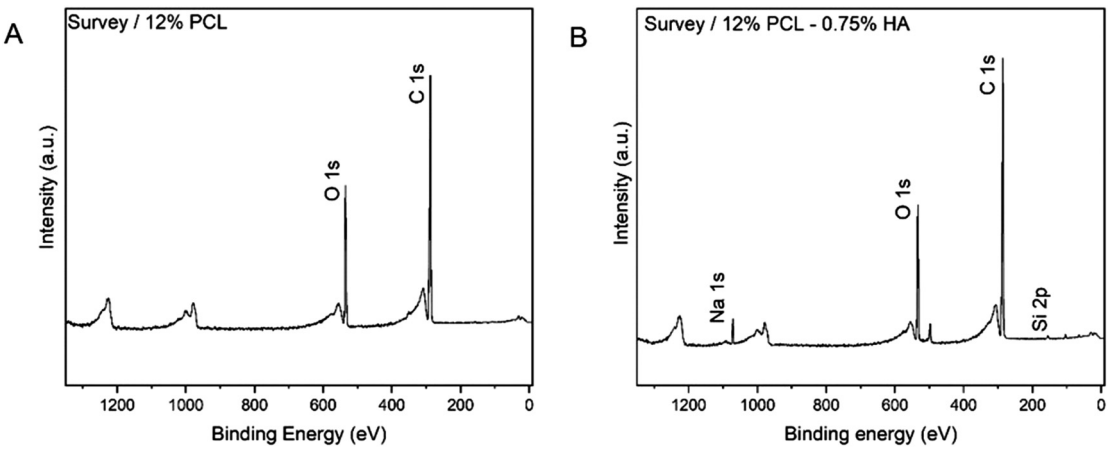

Fig. 6 XPS analysis. Elements present in the scaffold's surface. (A) 12% PCL scaffold. (B) 12% PCL 0.75% HA scaffold. PCL: polycaprolactone; HA: hyaluronic acid; O: oxygen; C: carbon; Na: sodium.

Open Access Article. Published on 31 July 2024. Downloaded on 10/30/2025 4:59:12 PM.
This article is licensed under a Creative Commons Attribution 3.0 Unported Licence.

In order to determine the impact of HA incorporation into the hydrophilic properties of the scaffolds, their contact angles were analyzed. As shown in Fig. 7, HA was able to decrease the hydrophobicity of PCL. When performing a three-way ANOVA statistical test, a HA concentration main effect with a p-value = 0.0091 and an alignment main effect with a p-value = 0.0021 were observed. PCL concentration did not show a main effect, but its interaction with HA concentration and alignment did, with p-values 0.0434 and 0.0294, respectively. Therefore, we conclude that HA concentration and alignment seemed to have an impact on reducing scaffold hydrophobicity.

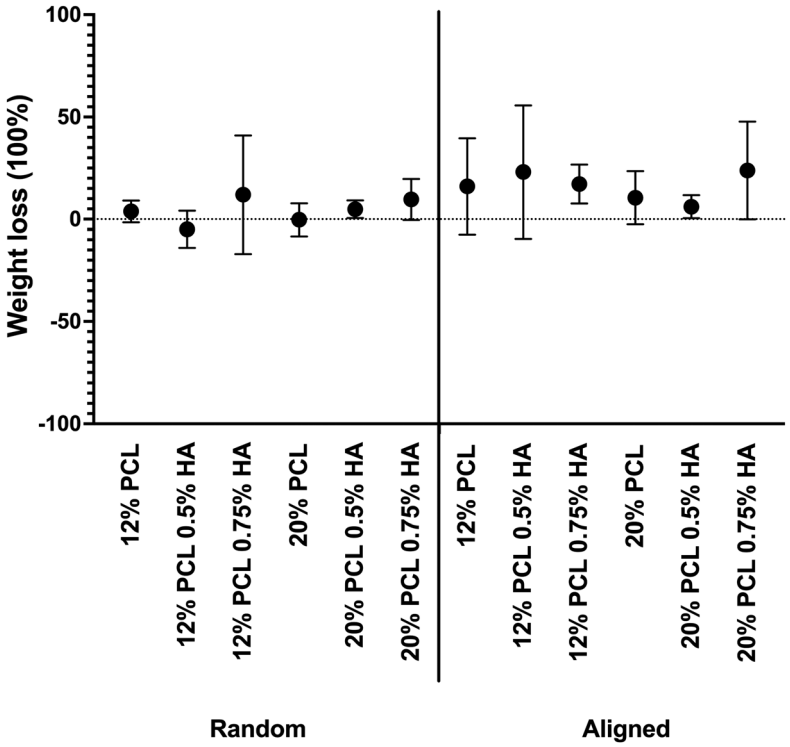

Fig. 8 Scaffold weight loss after 48 h of immersion in DMEM. PCL: polycaprolactone; HA: hyaluronic acid. Data are shown as mean ± SEM (n = 3).

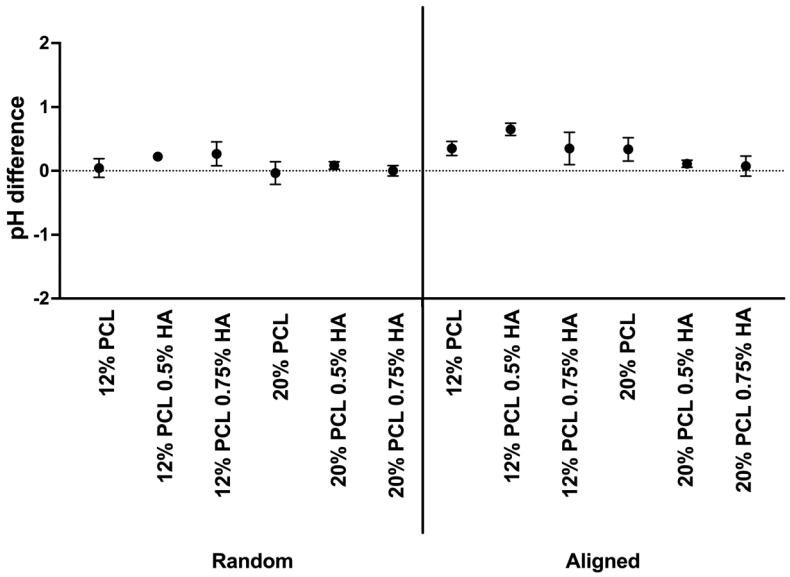

Fig. 9 pH variation in scaffolds after 48 h of immersion in DMEM. PCL: polycaprolactone; HA: hyaluronic acid. Data are shown as mean ± SEM (n = 3).

Open Access Article. Published on 31 July 2024. Downloaded on 10/30/2025 4:59:12 PM.
This article is licensed under a Creative Commons Attribution 3.0 Unported Licence.

3.3. Analyzing scaffold stability

The next step was to check the stability of the scaffolds in the very short term, as an innate immune response takes place in the first days after biomaterial implantation.[30,35] In order to analyze this parameter, the scaffold weight loss after 48 h immersion in DMEM, as well as the pH changes in the incubating medium, was measured.

As shown in Fig. 8, the samples did not show a weight loss, but some specimens showed an increase in this parameter.

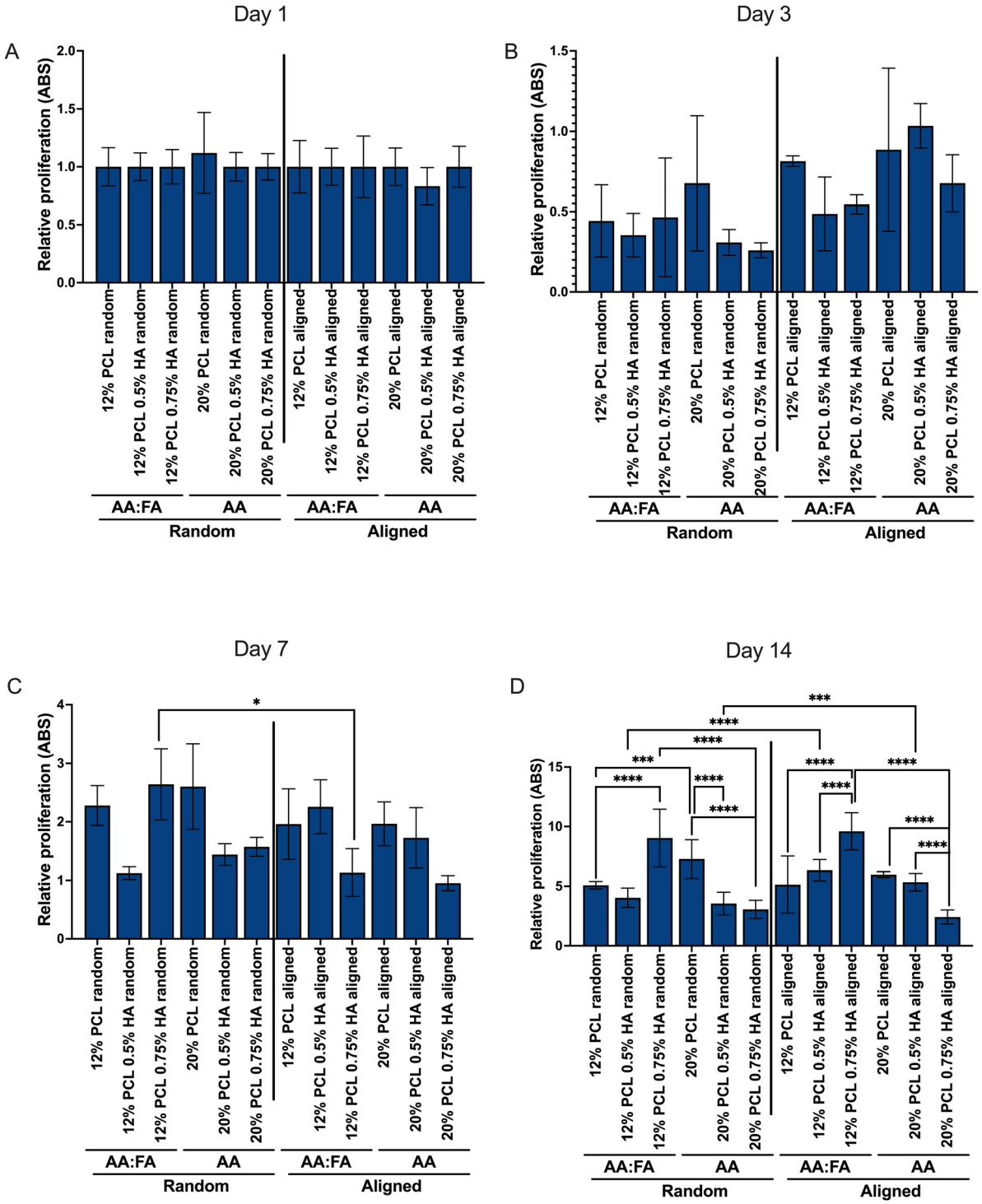

Fig. 10 NhDF proliferation. (A) Day 1; (B) day 3; (C) day 7; (D) day 14. PCL: polycaprolactone; HA: hyaluronic acid; AA: acetic acid; FA: formic acid; nm: nanometer. Data are shown as mean ± SEM (n = 3). Two-way ANOVA with $p^{*} < 0.05$; $p^{***} < 0.001$; $p^{****} < 0.0001$.

Open Access Article. Published on 31 July 2024. Downloaded on 10/30/2025 4:59:12 PM.
This article is licensed under a Creative Commons Attribution 3.0 Unported Licence.

Therefore, it was thought that the presence of salts and proteins in the DMEM might be the reason for such observable changes. Additionally, porosity might play a key role in this aspect by retaining medium and preventing scaffolds from drying out completely.

Alongside, Fig. 9 shows the pH variation. Samples showed less than 0.5 pH value variation, except for the 12% PCL 0.5% HA and the 12% PCL 0.75% HA aligned specimens. The latter showed a more basic medium than the control. This would correspond to no PCL degradation, as this process would release acidic by-products which would decrease the pH when reacting with water molecules.[71] Moreover, HA is known to degrade in short periods of time.[72] This process is highly dependent on the pH: between pH 4 to pH 11 degradation would not take place.[73] The DMEM used for the experiment showed a neutral pH, so no HA degradation was expected. Hence, according to these results, scaffolds were stable after 48 h.

3.4. NhDF proliferation and morphology

Although hydrophobicity was not affected by the incorporation of HA into the scaffolds, their cellular performance was assessed by means of NhDFs, in order to determine its influence as well as the influence of the scaffold's morphological features on cellular proliferation and morphology.

Fig. 10 shows the relative direct viability of NhDF in terms of absorbance (ABS) values, normalized against the first day after seeding them. It can be observed that cells at day 3 (Fig. 10B) showed a slightly lower absorbance than at day 1 (Fig. 10A). However, the proliferation of the cells increases subsequently, alongside for 2 weeks (Fig. 10C and D). In case the scaffolds were cytotoxic, proliferation of the cells would be prevented and cell numbers would decrease at day 7 and 14. Since the opposite effect was observed, we concluded that the scaffolds did not show a toxic effect and that the lower proliferation at day 3 might be due to the necessity of the cells adapt-

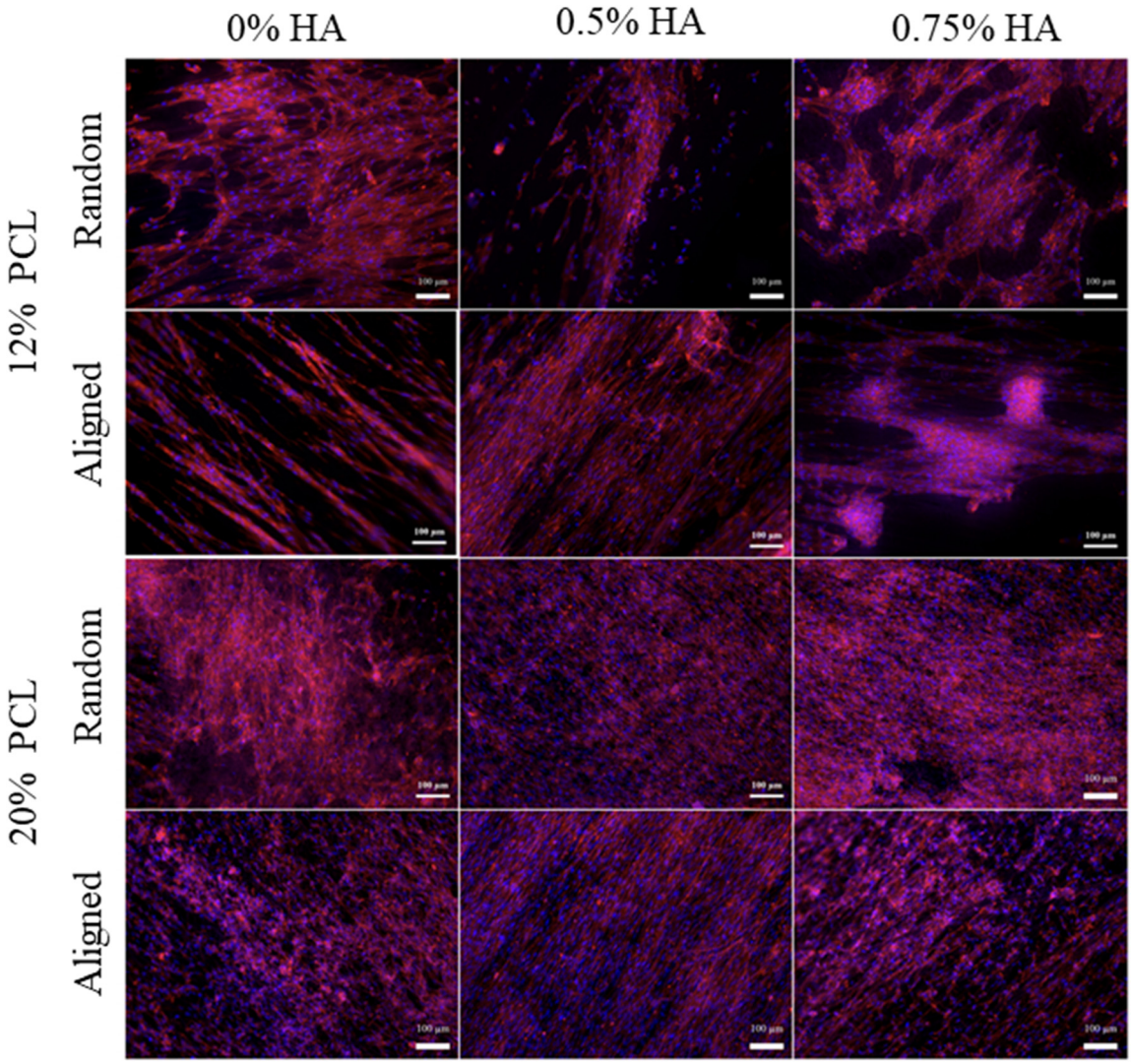

Fig. 11 NhDF morphology. Morphology of NhDF culured on top of the scaffolds for 1, 3, 7 and 14 days. NhDF cells were stained with DAPI and rhodamine-phalloidin.

Open Access Article. Published on 31 July 2024. Downloaded on 10/30/2025 4:59:12 PM.
This article is licensed under a Creative Commons Attribution 3.0 Unported Licence.

ing to the scaffold's presence. However, this should be further analyzed with viability tests such as LDH assay.

Additionally, beyond the first week of proliferation, differences between the different compositions could be observed. At day 14 (Fig. 10D), it can be observed that, independently of the fiber alignment, HA incorporation led to a higher proliferation when PCL concentration was lower (12%). However, for the higher PCL concentration (20%), the opposite effect was detected and, in general, the proliferation was lower when compared to the 12% PCL samples. As the HA integration was not having an impact on the hydrophilic properties, this phenomenon cannot be due to this latter parameter. However, HA was also impacting the fiber diameter and, as well, in an opposite way depending on the PCL concentration. For low PCL, the fiber diameter was increased when increasing HA concentration, while for 20% PCL specimens, the diameter decreased. Therefore, it seems that cellular proliferation is enhanced by fibers with higher diameter, a phenomenon already described for other polymer-based scaffolds and cell types.[60,62] Moreover, this event is even greater in the nanoscale, in comparison with the microscale, which is the general trend observed for this parameter.[61]

Concerning the spatial distribution of the fibers, differences between the different scaffolds were only observable at longer incubation times (Fig. 10D). Cells proliferated better in aligned specimens. Previous studies have described opposite effects of electrospun scaffold alignment on cell proliferation.[60,92] It seems that cell shape plays a key role in determining the ability of this alignment to improve their proliferation: the more the cell shape coincides with the alignment, as it occurs with keratocytes,[92] the greater proliferation. Therefore, the long, aligned shape of fibroblasts seems to favor their proliferation in aligned scaffolds.

When comparing the proliferation results with the porosity (Table 1), we can observe that, in general, the lower the pore, the better the proliferation. Previous studies have linked a higher porosity with a better cell growth.[84–86] However, in this study, except for the 20% PCL aligned scaffolds, the opposite effect was observed. As fiber diameter also has an impact on this parameter and the differences in this feature were more significant (Fig. 3), it can be said that the influence of the latter overcomes the pore size effect on cellular growth.

Fig. 11 shows the merge results from DAPI and rhodamine-phalloidin staining for day 7, chosen as the representative time point. Cells showed the expected morphology, which is a spindle shape and oval nucleus.[93] Additionally, as described in previous studies,[94,95] a better NhDF alignment in the aligned scaffolds could be observed.

3.5. Scaffold immune recognition by TLRs

In order to assess the effect of fiber diameter and alignment on immune recognition, different TLR reporter cell lines (TLR 4, TLR 2/1 and TLR 2/6)[64] were cultured in the presence of the different biomaterials for 24, 48 and 72 h. For both, viability and receptor stimulation level results, we observed no significant differences between the different time points.

According to the ISO 10993-5 standard on *Biological evaluation of medical devices*,[42] for negative cytotoxicity there should be at least an 80% viability. Results in Fig. 12 demonstrate that the viability of the three cell lines in contact with the 12 different compositions was 80% or higher. Therefore, it can be concluded that the biomaterials did not have cytotoxic effects on the TLR reporter cells.

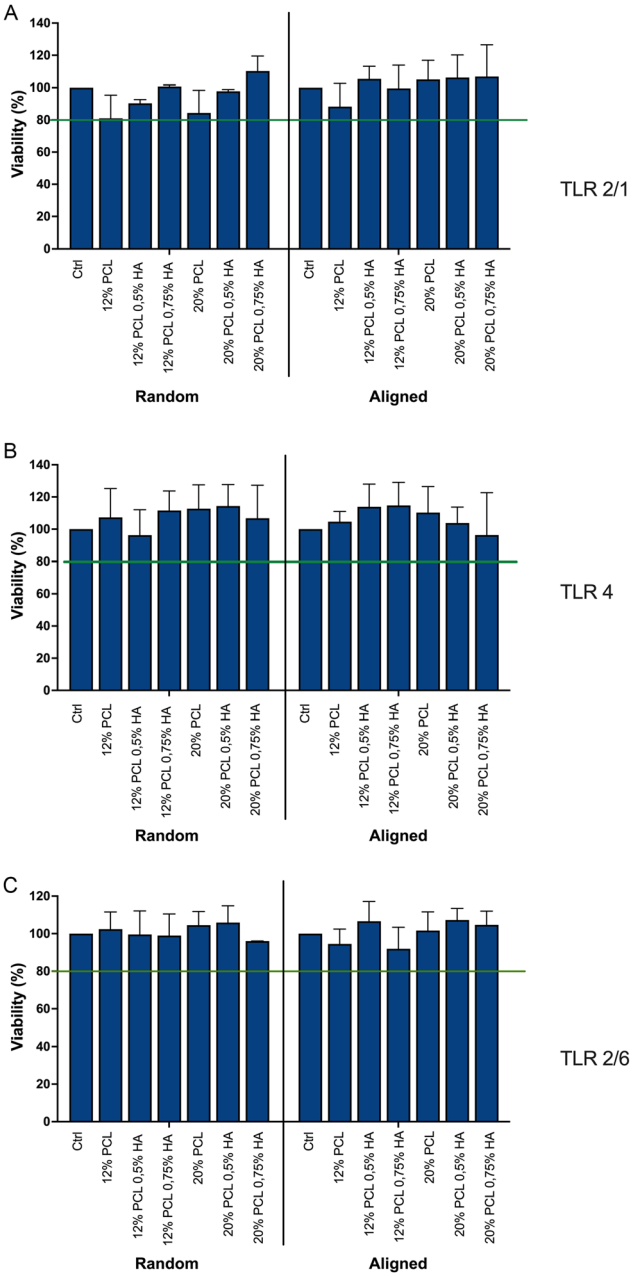

Fig. 12 TLR reporter cell line viability. Viability of TLRs is shown after being cultured for 24 h on top of the scaffolds. (A) TLR 2/1; (B) TLR 4; (C) TLR 6. PCL: polycaprolactone; HA: hyaluronic acid. Data are shown as mean ± SEM (n = 4). Threshold: 80% viability, according to ISO 10993-5.[42]

 This journal is © The Royal Society of Chemistry 2024

Open Access Article. Published on 31 July 2024. Downloaded on 10/30/2025 4:59:12 PM.
This article is licensed under a Creative Commons Attribution 3.0 Unported Licence.

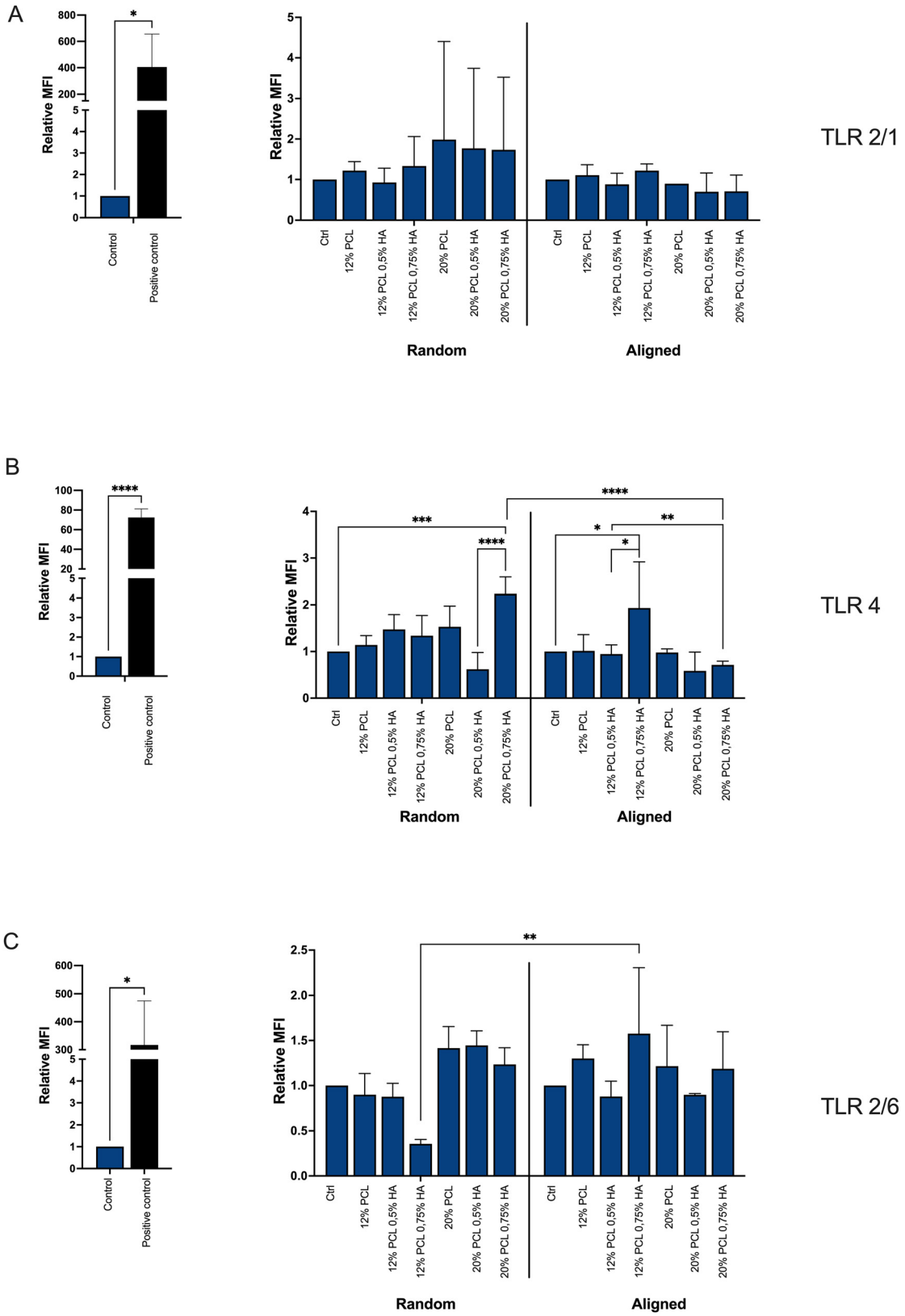

Fig. 13 Triggering of TLR reporters. Triggering of TLRs is shown after being cultured for 24 h on top of the scaffolds. (A) TLR 2/1; (B) TLR 4; (C) TLR 6. Positive control: activation upon culture in the presence of 100 nM phorbol 12-myristate 13-acetate, 12-*O*-tetradecanoylphorbol 13-acetate; PCL: polycaprolactone; HA: hyaluronic acid; MFI: mean fluorescence intensity. Data are shown as mean ± SEM (n = 4). Two-way ANOVA with $p^* < 0.05$; $p^{**} < 0.01$; $p^{***} < 0.001$; $p^{****} < 0.0001$.

Open Access Article. Published on 31 July 2024. Downloaded on 10/30/2025 4:59:12 PM.
This article is licensed under a Creative Commons Attribution 3.0 Unported Licence.

Regarding the activation of the TLRs, the biomaterials did not lead to the activation of neither TLR 2/1 (Fig. 13A) nor TLR 2/6 (Fig. 13C). However, TLR 4 was modestly triggered by the scaffolds with a higher percentage of HA (Fig. 13B). This stimulation was significant for the 20% PCL composition when fibers were randomly distributed, but not aligned; and for the 12% PCL specimen in the aligned group, but not the random one.

It seems that the higher the HA concentration, the more triggering of TLR 4 occurs, which can be explained by the low molecular weight of the HA applied, as it has been associated with inflammation.[96,97] However, the alignment of the fibers, as well as a higher concentration of PCL, seems to prevent this activation. It is known that plasma proteins adsorb on the biomaterial surface, exposing antigenic sites and initiating the recruitment of immune cells.[33] The alignment might reduce the accessibility of exposed antigenic sites of adsorbed proteins. Additionally, alignment may prevent direct interaction of the TLR with the biomaterial, which has been proposed for some biomaterials but not demonstrated before.[35,53] Regarding the PCL concentration, its increase reduces the HA/PCL ratio, which might lead to a less HA exposure and, therefore, less probabilities to induce inflammation.

4. Conclusions

In summary, our results show that higher PCL concentration enables obtaining electrospun fibers on the micrometer scale. Additionally, the incorporation of HA decreases the fiber diameter and hydrophobicity of the scaffolds, as well as improving the alignment of the fibers. Fibroblasts show a better proliferation in aligned scaffolds, favored by their elongated shape. Moreover, their growth shows an aligned distribution when cultured in aligned fibers. TLR 2/1 and TLR 2/6 are not triggered by the PCL–HA-based electrospun scaffolds. However, a higher concentration of HA leads to a modest TLR 4 stimulation. This triggering can be prevented by reducing the HA/PCL ratio and by the alignment of the fibers. Considering all the results, 12% PCL and 0.75% HA aligned scaffolds are considered to be the most promising ones, as the fiber diameter is within the nanometer scale, biomimicking the tendon native tissue structure, while additionally showing high alignment and hydrophilicity, leading to better cell proliferation and performance and a lower immunological recognition. Previous studies underlined the effect of the scaffold morphological features on macrophage polarization and native tendon cells. Our study demonstrated that scaffold morphology also impacts their recognition by TLRs, expressed on the surface of several innate immune cells (monocytes, neutrophils, dendritic cells and macrophages). The study of this biomaterial–immune system interplay is essential to predict the clinical outcome of biomaterial implantation. TLR 4, TLR 2/6 and TLR 2/1 are not the only TLRs expressed on the innate immune cells. Therefore, additional reporter cell lines should be investigated. Moreover, in spite of being one of the largest and most important PRR families, TLRs are not the only sensors involved in biomaterial recognition. Other receptors such as integrins or scavenger receptors should be also included in the *in vitro* analysis of biomaterial–immune system interplay. However, TLR reporter cell lines proved to be an excellent tool for further investigation in this regard, providing researchers with a cost-effective, simple, fast and easy read out system.

Author contributions

Design of the research was carried out by S. G. C., J. S. and A. R. B. S. G. C. performed the research, analysed the data and wrote the original draft. F. I., I. U. and V. P. provided experimental support. S. K. and C. W. provided technical support. F. K. performed the chemical composition analysis. K. A. R. and P. S. provided the reporter cell lines. S. G. C., F. I., I. U., S. K., V. P., J. S. and A. R. B. participated in the discussion of the results. J. S. and A. R. B supervised the work and provided resources, project administration and funding acquisition. All authors have reviewed the manuscript and given approval to the final version of the manuscript.

Conflicts of interest

There are no conflicts to declare.

Acknowledgements

This project has received funding from the European Union's Horizon 2020 research and innovation programme under the Marie Skłodowska-Curie grant agreement No 955685 (**https://www.p4fit.eu**).

References

1 G. Riley, Tendinopathy–from basic science to treatment, *Nat. Clin. Pract. Rheumatol.*, 2008, **4**(2), 82–89.
2 V. Russo, M. El Khatib, G. Prencipe, M. R. Citeroni, M. Faydaver, A. Mauro, *et al.* Tendon Immune Regeneration: Insights on the Synergetic Role of Stem and Immune Cells during Tendon Regeneration, *Cells*, 2022, **11**(3), 434.
3 D. T. Kirkendall and W. E. Garrett, Function and biomechanics of tendons, *Scand. J. Med. Sci. Sports*, 1997, **7**(2), 62–66.
4 M. R. Citeroni, M. C. Ciardulli, V. Russo, G. Della Porta, A. Mauro, M. El Khatib, *et al.*, In Vitro Innovation of Tendon Tissue Engineering Strategies, *Int. J. Mol. Sci.*, 2020, **21**(18), E6726.

 This journal is © The Royal Society of Chemistry 2024

Open Access Article. Published on 31 July 2024. Downloaded on 10/30/2025 4:59:12 PM.
This article is licensed under a Creative Commons Attribution 3.0 Unported Licence.

5 G. Crosio and A. H. Huang, Innate and adaptive immune system cells implicated in tendon healing and disease, *Eur. Cells Mater.*, 2022, **43**, 39–52.
6 J. Kastelic, A. Galeski and E. Baer, The multicomposite structure of tendon, *Connect. Tissue Res.*, 1978, **6**(1), 11–23.
7 M. Franchi, A. Trirè, M. Quaranta, E. Orsini and V. Ottani, Collagen structure of tendon relates to function, *Sci. World J.*, 2007, **7**, 404–420.
8 N. L. Millar, K. G. Silbernagel, K. Thorborg, P. D. Kirwan, L. M. Galatz, G. D. Abrams, *et al.* Tendinopathy, *Nat. Rev. Dis. Primers*, 2021, **7**(1), 1.
9 L. M. Dejardin, S. P. Arnoczky, B. J. Ewers, R. C. Haut and R. B. Clarke, Tissue-engineered rotator cuff tendon using porcine small intestine submucosa. Histologic and mechanical evaluation in dogs, *Am. J. Sports Med.*, 2001, **29**(2), 175–184.
10 J. Y. Sunwoo, C. D. Eliasberg, C. B. Carballo and S. A. Rodeo, The role of the macrophage in tendinopathy and tendon healing, *J. Orthop. Res.*, 2020, **38**(8), 1666–1675.
11 N. Maffulli, V. Barrass and S. W. Ewen, Light microscopic histology of achilles tendon ruptures. A comparison with unruptured tendons, *Am. J. Sports Med.*, 2000, **28**(6), 857–863.
12 N. Maffulli, S. W. Ewen, S. W. Waterston, J. Reaper and V. Barrass, Tenocytes from ruptured and tendinopathic achilles tendons produce greater quantities of type III collagen than tenocytes from normal achilles tendons. An in vitro model of human tendon healing, *Am. J. Sports Med.*, 2000, **28**(4), 499–505.
13 N. Andarawis-Puri, E. L. Flatow and L. J. Soslowsky, Tendon basic science: Development, repair, regeneration, and healing, *J. Orthop. Res.*, 2015, **33**(6), 780–784.
14 P. Sharma and N. Maffulli, Tendon injury and tendinopathy: healing and repair, *J. Bone Jt. Surg. Am.*, 2005, **87**(1), 187–202.
15 G. Walden, X. Liao, S. Donell, M. J. Raxworthy, G. P. Riley and A. Saeed, A Clinical, Biological, and Biomaterials Perspective into Tendon Injuries and Regeneration, *Tissue Eng., Part B*, 2017, **23**(1), 44–58.
16 V. Russo, M. El Khatib, G. Prencipe, A. Cerveró-Varona, M. R. Citeroni, A. Mauro, *et al.* Scaffold-Mediated Immunoengineering as Innovative Strategy for Tendon Regeneration, *Cells*, 2022, **11**(2), 266.
17 L. Battery and N. Maffulli, Inflammation in overuse tendon injuries, *Sports Med. Arthrosc. Rev.*, 2011, **19**(3), 213–217.
18 J. J. Green, Immunoengineering has arrived, *J. Biomed. Mater. Res., Part A*, 2021, **109**(4), 397–403.
19 T. Jiang, E. J. Carbone, K. W. H. Lo and C. T. Laurencin, Electrospinning of polymer nanofibers for tissue regeneration, *Prog. Polym. Sci.*, 2015, **46**, 1–24.
20 A. Repanas, S. Andriopoulou and B. Glasmacher, The significance of electrospinning as a method to create fibrous scaffolds for biomedical engineering and drug delivery applications, *J. Drug Delivery Sci. Technol.*, 2016, **31**, 137–146.
21 J. Xue, T. Wu, Y. Dai and Y. Xia, Electrospinning and Electrospun Nanofibers: Methods, Materials, and Applications, *Chem. Rev.*, 2019, **119**(8), 5298–5415.
22 S. Khorshidi, A. Solouk, H. Mirzadeh, S. Mazinani, J. M. Lagaron, S. Sharifi, *et al.*, A review of key challenges of electrospun scaffolds for tissue-engineering applications, *J. Tissue Eng. Regener. Med.*, 2016, **10**(9), 715–738.
23 A. Adamo, J. G. Bartolacci, D. D. Pedersen, M. G. Traina, S. Kim, A. Pantano, *et al.*, Continuous Microfiber Wire Mandrel–Less Biofabrication for Soft Tissue Engineering Applications, *Adv. Healthc. Mater.*, 2022, **11**(13), 2102613.
24 A. Chainani, K. J. Hippensteel, A. Kishan, N. W. Garrigues, D. S. Ruch, F. Guilak, *et al.*, Multilayered Electrospun Scaffolds for Tendon Tissue Engineering, *Tissue Eng., Part A*, 2013, **19**(23–24), 2594–2604.
25 A. Sensini, C. Gualandi, A. Zucchelli, L. A. Boyle, A. P. Kao, G. C. Reilly, *et al.* Tendon Fascicle-Inspired Nanofibrous Scaffold of Polylactic acid/Collagen with Enhanced 3D-Structure and Biomechanical Properties, *Sci. Rep.*, 2018, **8**(1), 17167.
26 Z. Najafi, P. Rahmanian-Devin, V. Baradaran Rahimi, A. Nokhodchi and V. R Askari, Challenges and opportunities of medicines for treating tendon inflammation and fibrosis: A comprehensive and mechanistic review, *Fundam. Clin. Pharmacol.*, 2024, e12999.
27 B. R. Freedman, D. J. Mooney and E. Weber, Advances toward transformative therapies for tendon diseases, *Sci. Transl. Med.*, 2022, **14**(661), eabl8814.
28 R. James, S. G. Kumbar, C. T. Laurencin, G. Balian and A. B. Chhabra, Tendon tissue engineering: adipose-derived stem cell and GDF-5 mediated regeneration using electrospun matrix systems, *Biomed. Mater.*, 2011, **6**(2), 025011.
29 E. Mariani, G. Lisignoli, R. M. Borzì and L. Pulsatelli, Biomaterials: Foreign Bodies or Tuners for the Immune Response?, *Int. J. Mol. Sci.*, 2019, **20**(3), 636.
30 A. Vishwakarma, N. S. Bhise, M. B. Evangelista, J. Rouwkema, M. R. Dokmeci, A. M. Ghaemmaghami, *et al.*, Engineering Immunomodulatory Biomaterials To Tune the Inflammatory Response, *Trends Biotechnol.*, 2016, **34**(6), 470–482.
31 J. M. Anderson, A. Rodriguez and D. T. Chang, Foreign body reaction to biomaterials, *Semin. Immunol.*, 2008, **20**(2), 86–100.
32 D. Salthouse, K. Novakovic, C. M. U. Hilkens and A. M. Ferreira, Interplay between biomaterials and the immune system: Challenges and opportunities in regenerative medicine, *Acta Biomater.*, 2023, **155**, 1–18.
33 F. J. Zhu, Y. L. Tong, Z. Y. Sheng and Y. M. Yao, Role of dendritic cells in the host response to biomaterials and their signaling pathways, *Acta Biomater.*, 2019, **94**, 132–144.
34 K. Wicherska-Pawłowska, T. Wróbel and J. Rybka, Toll-Like Receptors (TLRs), NOD-Like Receptors (NLRs), and RIG-I-Like Receptors (RLRs) in Innate Immunity. TLRs, NLRs, and RLRs Ligands as Immunotherapeutic Agents for Hematopoietic Diseases, *Int. J. Mol. Sci.*, 2021, **22**(24), 13397.

Open Access Article. Published on 31 July 2024. Downloaded on 10/30/2025 4:59:12 PM.
This article is licensed under a Creative Commons Attribution 3.0 Unported Licence.

35 R. J. Love and K. S. Jones, The recognition of biomaterials: pattern recognition of medical polymers and their adsorbed biomolecules, *J. Biomed. Mater. Res., Part A*, 2013, **101**(9), 2740–2752.
36 H. Chen, D. K. Agrawal and F. G. Thankam, Biomaterials-Driven Sterile Inflammation, *Tissue Eng., Part B*, 2022, **28**(1), 22–34.
37 S. Wang, Y. Chen, Z. Ling, J. Li, J. Hu, F. He, *et al.*, The role of dendritic cells in the immunomodulation to implanted biomaterials, *Int. J. Oral Sci.*, 2022, **14**(1), 52.
38 C. Blum, M. B. Taskin, J. Shan, T. Schilling, K. Schlegelmilch, J. Teßmar, *et al.* Appreciating the First Line of the Human Innate Immune Defense: A Strategy to Model and Alleviate the Neutrophil Elastase–Mediated Attack toward Bioactivated Biomaterials, *Small*, 2021, **17**(13), 2007551.
39 A. S. Tripathi, M. E. A. Zaki, S. A. Al-Hussain, B. K. Dubey, P. Singh, L. Rind, *et al.* Material matters: exploring the interplay between natural biomaterials and host immune system, *Front. Immunol.*, 2023, **14**, 1269960.
40 N. Bian, C. Chu, S. Rung, V. Huangphattarakul, Y. Man, J. Lin, *et al.*, Immunomodulatory Biomaterials and Emerging Analytical Techniques for Probing the Immune Micro-Environment, *Tissue Eng. Regener. Med.*, 2023, **20**(1), 11–24.
41 A. Lock, J. Cornish and D. S. Musson, The Role of In Vitro Immune Response Assessment for Biomaterials, *J. Funct. Biomater.*, 2019, **10**(3), 31.
42 B. Iso and B. Standard, *Biological evaluation of medical devices, Part 1*, 2009, p. 10993.
43 G. Hulsart-Billström, J. I. Dawson, S. Hofmann, R. Müller, M. J. Stoddart, M. Alini, *et al.* A surprisingly poor correlation between in vitro and in vivo testing of biomaterials for bone regeneration: results of a multicentre analysis, *Eur. Cells Mater.*, 2016, **31**, 312–322.
44 A. Cipitria, A. Skelton, T. R. Dargaville, P. D. Dalton and D. W. Hutmacher, Design, fabrication and characterization of PCL electrospun scaffolds—a review, *J. Mater. Chem.*, 2011, **21**(26), 9419.
45 N. Siddiqui, S. Asawa, B. Birru, R. Baadhe and S. Rao, PCL-Based Composite Scaffold Matrices for Tissue Engineering Applications, *Mol. Biotechnol.*, 2018, **60**(7), 506–532.
46 G. Yang, H. Lin, B. B. Rothrauff, S. Yu and R. S. Tuan, Multilayered polycaprolactone/gelatin fiber-hydrogel composite for tendon tissue engineering, *Acta Biomater.*, 2016, **35**, 68–76.
47 H. Ehtesabi and F. Massah, Improvement of hydrophilicity and cell attachment of polycaprolactone scaffolds using green synthesized carbon dots, *Mater. Today Sustain.*, 2021, **13**, 100075.
48 W. Wang, G. Caetano, W. S. Ambler, J. J. Blaker, M. A. Frade, P. Mandal, *et al.* Enhancing the Hydrophilicity and Cell Attachment of 3D Printed PCL/Graphene Scaffolds for Bone Tissue Engineering, *Materials*, 2016, **9**(12), 992.
49 H. S. Kim, S. G. Kumbar and S. P. Nukavarapu, Biomaterial-directed cell behavior for tissue engineering, *Curr. Opin. Biomed. Eng.*, 2021, **17**, 100260.
50 D. F. Moyano, M. Goldsmith, D. J. Solfiell, D. Landesman-Milo, O. R. Miranda, D. Peer, *et al.*, Nanoparticle hydrophobicity dictates immune response, *J. Am. Chem. Soc.*, 2012, **134**(9), 3965–3967.
51 M. M. Ouberai, K. Xu and M. E. Welland, Effect of the interplay between protein and surface on the properties of adsorbed protein layers, *Biomaterials*, 2014, **35**(24), 6157–6163.
52 S. Hamlet, M. Alfarsi, R. George and S. Ivanovski, The effect of hydrophilic titanium surface modification on macrophage inflammatory cytokine gene expression, *Clin. Oral Implants Res.*, 2012, **23**(5), 584–590.
53 F. Batool, H. Özçelik, C. Stutz, P. Y. Gegout, N. Benkirane-Jessel, C. Petit, *et al.*, Modulation of immune-inflammatory responses through surface modifications of biomaterials to promote bone healing and regeneration, *J. Tissue Eng.*, 2021, **12**, 20417314211041428.
54 K. M. Hotchkiss, G. B. Reddy, S. L. Hyzy, Z. Schwartz, B. D. Boyan and R. Olivares-Navarrete, Titanium surface characteristics, including topography and wettability, alter macrophage activation, *Acta Biomater.*, 2016, **31**, 425–434.
55 C. Chircov, A. M. Grumezescu and L. E. Bejenaru, Hyaluronic acid-based scaffolds for tissue engineering, *Rom. J. Morphol. Embryol.*, 2018, **59**(1), 71–76.
56 C. L. Romanò, E. De Vecchi, M. Bortolin, I. Morelli and L. Drago, Hyaluronic Acid and Its Composites as a Local Antimicrobial/Antiadhesive Barrier, *J. Bone Jt. Infect.*, 2017, **2**(1), 63–72.
57 L. Osti, M. Berardocco, V. di Giacomo, G. Di Bernardo, F. Oliva and A. C. Berardi, Hyaluronic acid increases tendon derived cell viability and collagen type I expression in vitro: Comparative study of four different Hyaluronic acid preparations by molecular weight, *BMC Musculoskeletal Disord.*, 2015, **16**(1), 284.
58 S. Wu, H. Peng, X. Li, P. N. Streubel, Y. Liu and B. Duan, Effect of scaffold morphology and cell co-culture on tenogenic differentiation of HADMSC on centrifugal melt electrospun poly (L-lactic acid) fibrous meshes, *Biofabrication*, 2017, **9**(4), 044106.
59 X. Li, X. Wang, D. Yao, J. Jiang, X. Guo, Y. Gao, *et al.*, Effects of aligned and random fibers with different diameter on cell behaviors, *Colloids Surf., B*, 2018, **171**, 461–467.
60 A. S. Badami, M. R. Kreke, M. S. Thompson, J. S. Riffle and A. S. Goldstein, Effect of fiber diameter on spreading, proliferation, and differentiation of osteoblastic cells on electrospun poly(lactic acid) substrates, *Biomaterials*, 2006, **27**(4), 596–606.
61 E. Martínez, E. Engel, J. A. Planell and J. Samitier, Effects of artificial micro- and nano-structured surfaces on cell behaviour, *Ann. Anat. – Ann. Anat.*, 2009, **191**(1), 126–135.
62 L. Moroni, R. Licht, J. De Boer, J. R. De Wijn and C. A. Van Blitterswijk, Fiber diameter and texture of electrospun

 This journal is © The Royal Society of Chemistry 2024

Open Access Article. Published on 31 July 2024. Downloaded on 10/30/2025 4:59:12 PM. This article is licensed under a Creative Commons Attribution 3.0 Unported Licence.

PEOT/PBT scaffolds influence human mesenchymal stem cell proliferation and morphology, and the release of incorporated compounds, *Biomaterials*, 2006, **27**(28), 4911–4922.

63 S. Jutz, A. Hennig, W. Paster, Ö. Asrak, D. Dijanovic, F. Kellner, *et al.*, A cellular platform for the evaluation of immune checkpoint molecules, *Oncotarget*, 2017, **8**(39), 64892–64906.

64 K. Radakovics, C. Battin, J. Leitner, S. Geiselhart, W. Paster, J. Stöckl, *et al.*, A Highly Sensitive Cell-Based TLR Reporter Platform for the Specific Detection of Bacterial TLR Ligands, *Front. Immunol.*, 2021, **12**, 817604.

65 C. H. Chen, D. L. Li, A. D. C. Chuang, B. S. Dash and J. P. Chen, Tension Stimulation of Tenocytes in Aligned Hyaluronic Acid/Platelet-Rich Plasma-Polycaprolactone Core-Sheath Nanofiber Membrane Scaffold for Tendon Tissue Engineering, *Int. J. Mol. Sci.*, 2021, **22**(20), 11215.

66 E. Entekhabi, M. H. Nazarpak, F. Moztarzadeh and A. Sadeghi, Design and manufacture of neural tissue engineering scaffolds using hyaluronic acid and polycaprolactone nanofibers with controlled porosity, *Mater. Sci. Eng., C*, 2016, **69**, 380–387.

67 S. Jiang, H. Yan, D. Fan, J. Song and C. Fan, Multi-layer electrospun membrane mimicking tendon sheath for prevention of tendon adhesions, *Int. J. Mol. Sci.*, 2015, **16**(4), 6932–6944.

68 S. M. Khatami, K. Parivar, A. N. Sohi, M. Soleimani and H. Hanaee-Ahvaz, Acetylated hyaluronic acid effectively enhances chondrogenic differentiation of mesenchymal stem cells seeded on electrospun PCL scaffolds, *Tissue Cell*, 2020, **65**, 101363.

69 D. Rachmiel, I. Anconina, S. Rudnick-Glick, M. Halperin-Sternfeld, L. Adler-Abramovich and A. Sitt, Hyaluronic Acid and a Short Peptide Improve the Performance of a PCL Electrospun Fibrous Scaffold Designed for Bone Tissue Engineering Applications, *Int. J. Mol. Sci.*, 2021, **22**(5), 2425.

70 S. Unal, S. Arslan, B. K. Yilmaz, F. N. Oktar, D. Ficai, A. Ficai, *et al.* Polycaprolactone/Gelatin/Hyaluronic Acid Electrospun Scaffolds to Mimic Glioblastoma Extracellular Matrix, *Materials*, 2020, **13**(11), E2661.

71 E. Widiatmoko, M. Abdullah and K. Khairurrijal, A Method to Measure Pore Size Distribution of Porous Materials Using Scanning Electron Microscopy Images, *AIP Conf. Proc.*, 2010, **1284**, 23–26.

72 A. A. M. Zubir, M. P. Khairunnisa, N. A. Surib, J. NorRuwaida, A. H. B. M. Ali and M. Rashid, Electrospinning of PLA with DMF: Effect of polymer concentration on the bead diameter of the electrospun fibre, *IOP Conf. Ser.: Mater. Sci. Eng.*, 2020, **778**(1), 012087.

73 H. Maleki, A. A. Gharehaghaji, L. Moroni and P. J. Dijkstra, Influence of the solvent type on the morphology and mechanical properties of electrospun PLLA yarns, *Biofabrication*, 2013, **5**(3), 035014.

74 A. Haider, S. Haider and I. K. Kang, A comprehensive review summarizing the effect of electrospinning parameters and potential applications of nanofibers in biomedical and biotechnology, *Arabian J. Chem.*, 2018, **11**(8), 1165–1188.

75 W. M. Haynes, D. R. Lide and T. J. Bruno, CRC Handbook of Chemistry and Physics, in *Occup. Environ. Med.*, 76th edn, 1996.

76 C. J. Angammana and S. H. Jayaram, Analysis of the Effects of Solution Conductivity on Electrospinning Process and Fiber Morphology, *IEEE Trans. Ind. Appl.*, 2011, **47**(3), 1109–1117.

77 X. Zong, K. Kim, D. Fang, S. Ran, B. S. Hsiao and B. Chu, Structure and process relationship of electrospun bioabsorbable nanofiber membranes, *Polymer*, 2002, **43**(16), 4403–4412.

78 J. S. Choi, S. W. Lee, L. Jeong, S. H. Bae, B. C. Min, J. H. Youk, *et al.* Effect of organosoluble salts on the nanofibrous structure of electrospun poly(3-hydroxybutyrate-co-3-hydroxyvalerate), *Int. J. Biol. Macromol.*, 2004, **34**(4), 249–256.

79 A. Chanda, J. Adhikari, A. Ghosh, S. R. Chowdhury, S. Thomas, P. Datta, *et al.* Electrospun chitosan/polycaprolactone-hyaluronic acid bilayered scaffold for potential wound healing applications, *Int. J. Biol. Macromol.*, 2018, **116**, 774–785.

80 M. Lebourg, S. Martínez-Díaz, N. García-Giralt, R. Torres-Claramunt, J. G. Ribelles, G. Vila-Canet, *et al.* Cell-free cartilage engineering approach using hyaluronic acid–polycaprolactone scaffolds: A study *in vivo*, *J. Biomater. Appl.*, 2014, **28**(9), 1304–1315.

81 A. J. Robinson, A. Pérez-Nava, S. C. Ali, J. B. González-Campos, J. L. Holloway and E. M. Cosgriff-Hernandez, Comparative Analysis of Fiber Alignment Methods in Electrospinning, *Matter*, 2021, **4**(3), 821–844.

82 M. A. Alfaro De Prá, R. M. Ribeiro-do-Valle, M. Maraschin and B. Veleirinho, Effect of collector design on the morphological properties of polycaprolactone electrospun fibers, *Mater. Lett.*, 2017, **193**, 154–157.

83 R. M. Nezarati, M. B. Eifert and E. Cosgriff-Hernandez, Effects of Humidity and Solution Viscosity on Electrospun Fiber Morphology, *Tissue Eng., Part C*, 2013, **19**(10), 810–819.

84 E. Bianchi, M. Ruggeri, S. Rossi, B. Vigani, D. Miele, M. C. Bonferoni, *et al.* Innovative Strategies in Tendon Tissue Engineering, *Pharmaceutics*, 2021, **13**(1), 89.

85 Y. X. Liu, F. J. Chaparro, Z. Tian, Y. Jia, J. Gosser, J. Gaumer, *et al.* Visualization of porosity and pore size gradients in electrospun scaffolds using laser metrology, *PLoS One*, 2023, **18**(3), e0282903.

86 T. Dai, J. Ma, S. Ni, C. Liu, Y. Wang, S. Wu, *et al.*, Attapulgite-doped electrospun PCL scaffolds for enhanced bone regeneration in rat cranium defects, *Biomater. Adv.*, 2022, **133**, 112656.

87 M. N. Collins and C. Birkinshaw, Hyaluronic acid based scaffolds for tissue engineering—A review, *Carbohydr. Polym.*, 2013, **92**(2), 1262–1279.

88 M. Essendoubi, C. Gobinet, R. Reynaud, J. F. Angiboust, M. Manfait and O. Piot, Human skin penetration of hya-

Open Access Article. Published on 31 July 2024. Downloaded on 10/30/2025 4:59:12 PM.
This article is licensed under a Creative Commons Attribution 3.0 Unported Licence.

luronic acid of different molecular weights as probed by Raman spectroscopy, *Skin Res. Technol.*, 2016, **22**(1), 55–62.

89 S. Manju and K. Sreenivasan, Conjugation of curcumin onto hyaluronic acid enhances its aqueous solubility and stability, *J. Colloid Interface Sci.*, 2011, **359**(1), 318–325.

90 A. M. Vasi, M. I. Popa, M. Butnaru, G. Dodi and L. Verestiuc, Chemical functionalization of hyaluronic acid for drug delivery applications, *Mater. Sci. Eng., C*, 2014, **38**, 177–185.

91 Y. C. Huang, K. Y. Huang, W. Z. Lew, K. H. Fan, W. J. Chang and H. M. Huang, Gamma-Irradiation-Prepared Low Molecular Weight Hyaluronic Acid Promotes Skin Wound Healing, *Polymers*, 2019, **11**(7), 1214.

92 J. Yan, L. Qiang, Y. Gao, X. Cui, H. Zhou, S. Zhong, *et al.* Effect of fiber alignment in electrospun scaffolds on keratocytes and corneal epithelial cells behavior, *J. Biomed. Mater. Res., Part A*, 2012, **100**(2), 527–535.

93 U. Lendahl, L. Muhl and C. Betsholtz, Identification, discrimination and heterogeneity of fibroblasts, *Nat. Commun.*, 2022, **13**(1), 3409.

94 C. J. Lowe, I. M. Reucroft, M. C. Grota and D. I. Shreiber, Production of Highly Aligned Collagen Scaffolds by Freeze-drying of Self-assembled, Fibrillar Collagen Gels, *ACS Biomater. Sci. Eng.*, 2016, **2**(4), 643–651.

95 Q. Xing, C. Vogt, K. W. Leong and F. Zhao, Highly Aligned Nanofibrous Scaffold Derived from Decellularized Human Fibroblasts, *Adv. Funct. Mater.*, 2014, **24**(20), 3027–3035.

96 A. Marinho, C. Nunes and S. Reis, Hyaluronic Acid: A Key Ingredient in the Therapy of Inflammation, *Biomolecules*, 2021, **11**(10), 1518.

97 R. Altman, A. Bedi, A. Manjoo, F. Niazi, P. Shaw and P. Mease, Anti-Inflammatory Effects of Intra-Articular Hyaluronic Acid: A Systematic Review, *Cartilage*, 2019, **10**(1), 43–52.

 This journal is © The Royal Society of Chemistry 2024